

Design of an ion trap for trapping single $^{171}\text{Yb}^+$

S. De, N. Batra, S. Chakraborty, S. Panja and A. Sen Gupta

We present an ion trap design of end-cap geometry and numerically calculate its potential. An rf-resonator of quality factor 800(20) has been fabricated for delivering high voltage to the trap. An optical frequency standard will be developed by trapping and laser cooling a single $^{171}\text{Yb}^+$. Optical arrangements for photoionization, laser cooling and detection are also described.

We are in an era where requirement of highly accurate time is becoming a necessity in diverse fields. With modern technological advances, clocks with accuracy of 10^{-9} sec are routinely used in satellite-based navigation, satellite tracking, high-speed telecommunication, geophysical experiments and elsewhere. Requirements of accuracy in time or frequency are more stringent for testing some fundamental theories in physical sciences. For example, temporal constancy of some constants such as fine structure constant α (refs 1 and 2) and electron-to-proton mass ratio m_e/m_p (ref. 3) is yet to be established. Such experimental verifications would require multiple clocks at different places with accuracy better than 10^{-18} sec. Test of general relativity using ultra-sensitive clocks is another aspect, e.g. dependence of transition rates in atomic clocks on solar gravitational potential has been reported^{4,5}. So far the primary frequency standards have relied on the microwave excitation of ^{133}Cs atoms between them doubly split hyperfine ground states. In SI unit ‘one second’ is defined as the time required for 9,192,631,770 cycles between two hyperfine ground states of ^{133}Cs atoms⁶. A microwave frequency standard has so far achieved its best fractional systematic accuracy $\Delta\nu/\nu = 2.1 \times 10^{-16}$ in ^{133}Cs -fountain clock⁷. The Allan deviation⁸ reduces significantly when a frequency standard operates in the optical wavelengths. The hyperfine induced $^1\text{S}_0$ - $^3\text{P}_0$ ultra-narrow transitions in neutral atoms⁹, trapped in suitable optical lattices¹⁰ are attractive for frequency standards, since $J = 0$ states are free from electric quadrupole shifts. As for example, ^{199}Hg (ref. 11), ^{171}Yb (ref. 12), ^{87}Sr (ref. 13) and ^{40}Ca (ref. 14) have already been demonstrated as secondary frequency standards with $\Delta\nu/\nu < 10^{-17}$.

Optical frequency standards with a single trapped ion provides long-term stability since they are free from inter-

ionic Coulomb and intra-atomic interactions. Trapped ion optical frequency standards have already been established with $^{199}\text{Hg}^+$, $^{171}\text{Yb}^+$, $^{88}\text{Sr}^+$, $^{40}\text{Ca}^+$, $^{115}\text{In}^+$ and $^{27}\text{Al}^+$. The $^{199}\text{Hg}^+$ clock operates at wavelength 282 nm, driving the $|^2\text{S}_{1/2}; F=0; m_F=0\rangle - |^2\text{D}_{5/2}; F=2; m_F=0\rangle$ electric quadrupole transition (E2) having a natural line-width of 1.8 Hz. For $^{199}\text{Hg}^+$ a fractional accuracy $\Delta\nu/\nu = 1.9 \times 10^{-17}$ at frequency $\nu = 1\,064\,721\,609\,899\,143$ Hz is reported by NIST, USA². The $^{171}\text{Yb}^+$ has three ultra-narrow transitions. Of these the $|^2\text{S}_{1/2}; F=0; m_F=0\rangle - |^2\text{D}_{3/2}; F=2; m_F=0\rangle$ E2-transition at wavelength 435.5 nm has natural line-width 3.02 Hz. This serves frequency standards at $\nu = 688\,358\,979\,309\,306.62$ Hz with $\Delta\nu/\nu = 5 \times 10^{-16}$ reported by PTB, Germany¹⁵. The $|^2\text{S}_{1/2}; F=0; m_F=0\rangle - |^2\text{F}_{7/2}; F=3; m_F=0\rangle$ electric octupole transition (E3) at wavelength 467 nm has natural line-width 1 nHz. The frequency shifts in an electric field gradient are higher at the $^2\text{D}_{3/2}$ -state than at the $^2\text{F}_{7/2}$ -state due to their electric quadrupole moments $2.08(11)ea_0^2$ (ref. 16) and $-0.041(5)ea_0^2$ (ref. 17) respectively, where e is electronic charge and a_0 is Bohr radius. The clock at $\nu = 642\,121\,496\,772\,645.15$ Hz E3-transition provides $\Delta\nu/\nu = 7.1 \times 10^{-17}$ as reported by PTB, Germany¹⁷. The $^{88}\text{Sr}^+$ clock operates at the wavelength 674 nm, which drives the $^2\text{S}_{1/2}$ - $^2\text{D}_{5/2}$ transition of natural line-width 0.4 Hz. There $\Delta\nu/\nu = 2.3 \times 10^{-17}$ is reported at $\nu = 444\,779\,044\,095\,485.5$ Hz by NRC, Canada¹⁸. The frequency $411\,042\,129\,776\,393.0$ Hz of the $^2\text{S}_{1/2}$ - $^2\text{D}_{5/2}$ E2-transition at wavelength 729 nm in $^{40}\text{Ca}^+$ has been reported with $\Delta\nu/\nu = 6.5 \times 10^{-16}$ by the CAS, China¹⁹. However, due to unavailability of magnetic field-insensitive energy levels in $^{88}\text{Sr}^+$ and $^{40}\text{Ca}^+$, the clocks are sensitive to the first-order Zeeman shifts. The hyperfine induced transitions at the wavelengths 237 and 267 nm in $^{115}\text{In}^+$ and $^{27}\text{Al}^+$ are attractive for clocks due to

higher frequency. For $^{115}\text{In}^+$, $\Delta\nu/\nu = 2.35 \times 10^{-13}$ at $\nu = 1\,267\,402\,452\,899\,920$ Hz has been reported by MPQ, Germany²⁰. The $^{27}\text{Al}^+$ clock at $\nu = 1\,121\,015\,393\,207\,851$ Hz has been reported as the most accurate ion clock with an accuracy $\Delta\nu/\nu = 8.6 \times 10^{-18}$ by NIST, USA²¹. Lasers at the deep UV wavelength, sympathetic cooling and special techniques to minimize the magnetic field sensitivity require heroic efforts for building $^{115}\text{In}^+$ and $^{27}\text{Al}^+$ clocks. There are few more ions proposed to serve as optical frequency standards. For example, the $|^2\text{S}_{1/2}; F=4; m_F=0\rangle - |^2\text{D}_{5/2}; F=6; m_F=0\rangle$ transition at wavelength 729 nm in $^{43}\text{Ca}^+$ (ref. 22) and the $|^2\text{S}_{1/2}; F=2; m_F=0\rangle - |^2\text{D}_{3/2}; F=0; m_F=0\rangle$ transition at wavelength 828 nm in $^{223}\text{Ra}^+$ (ref. 23) are under development.

At CSIR-NPL, New Delhi we are building an optical frequency standard using the $|^2\text{S}_{1/2}; F=0; m_F=0\rangle - |^2\text{F}_{7/2}; F=3; m_F=0\rangle$ E3-transition of $^{171}\text{Yb}^+$. The $m_F=0$ energy levels associated to the clock transitions are insensitive to the first-order Zeeman shifts. The states associated with the E3-transition have sensitivity -5.95 for measuring the temporal constancy of α (ref. 24), which is three orders of magnitude higher than in $^{27}\text{Al}^+$ (ref. 25). In this article we describe the design of our ion trap and the associated optical set-ups.

Experimental set-up

The trapped ion optical frequency standard set-up consists of an ion trap placed inside of an ultra high vacuum (UHV), optical arrangement of five lasers, detection of the single ion and stabilizing the clock laser at sub-Hz line-width. In the following subsections we shall describe the ion trap design, characterize its confining potential, parameters of the fabricated rf-resonator and the optical arrangements for laser cooling the ion.

Ion trap

Confinement of an ion carrying charge Q requires electric field (Paul trap)²⁶ or combination of electric and magnetic fields (Penning trap)²⁷. The Paul trap requires combination of a static U and oscillating $V\cos\omega_{\text{rf}}t$ electric fields to alter the local minima of the potential $\Phi(x, y, z, t)$ along the radial and axial directions²⁸. The ion remains trapped in 3D since the driving frequency ω_{rf} is much faster than the motion of the ion. The force experienced by the ion of mass m is

$$m\ddot{\mathbf{r}} = -Q\nabla\Phi(x, y, z, t), \quad (1)$$

where \mathbf{r} is the position vector of the ion with respect to the point where the force vanishes. A harmonic potential is desired since the restoring force increases linearly in all directions from the centre of the trap. An appropriate linear combination of electric fields $V_{\text{T}}(t) = U + V\cos\omega_{\text{rf}}t$ could produce a nearly harmonic potential

$$\Phi(x, y, z, t) = \frac{V_{\text{T}}(t)}{2R^2}(\alpha x^2 + \beta y^2 + \gamma z^2), \quad (2)$$

where α, β, γ determine curvatures of Φ in the respective directions and R is the radius of the trap volume, determined by distances between trap electrodes. Laplace's equation $\Delta\Phi(x, y, z, t) = 0$ constrains the coefficients to satisfy $\alpha + \beta + \gamma = 0$. A linear trap with $\alpha = -\beta = 1$ and $\gamma = 0$ is a good choice for trapping chain ions since the axial confinement is shallow. For trapping single ion, cylindrically symmetric trap is more preferable. In that case the choice of the coefficients is $\alpha = \beta = 1, \gamma = -2$. Several geometries of ion traps with cylindrical symmetry have been tried such as hyperbolic²⁹, ring³⁰ and end-cap³¹ traps. Hyperbolic trap would be the ideal choice for producing a pure quadrupole potential, but it provides very little access to the trap centre for lights and for ion source. The optical access to the centre is better for the ring trap, but is still somewhat limited. We have opted for the end-cap trap geometry due to its most optimal access for the required five laser beams and the Yb-atomic beam.

In practice, $\Phi(x, y, z, t)$ has always anharmonic contribution due to imperfect

alignment of the electrodes or tolerance in machining. The perturbation from a pure quadrupole field can be estimated from multipoles of order k , where $k = 0$ (monopole), 1 (dipole), 2 (quadrupole), 3 (hexapole), 4 (octupole) and so on. The generalized form of the potential is

$$\Phi = V_{\text{T}}(t) \sum_{l=0}^{\infty} \sum_{m=-l}^l a_{lm} \sqrt{\frac{(l-m)!}{(l+m)!}} \left(\frac{r}{R}\right)^l \times P_l^m(\cos\theta) e^{im\phi}, \quad (3)$$

where a_{lm} are coefficients of the corresponding multipole of order $k = l$, $P_l^m(\cos\theta)$ are associated Legendre polynomials and θ, ϕ are azimuthal and polar angles respectively. Due to symmetry in the trap geometry, the odd-order multipoles do not contribute. Only even m contribute due to the inversion symmetry in the radial plane. The quadrupole potential is

$$\Phi^{(2)} = -\Phi_0^{(2)}[(1-\varepsilon)x^2 + (1+\varepsilon)y^2 - 2z^2], \quad (4)$$

where $\Phi_0^{(2)} = V_{\text{T}}(t)a_{20}/2R^2$ and $\varepsilon = \sqrt{6}a_{22}/a_{20}$. Among the non-vanishing higher orders, the octupole potential leads to the dominant perturbation of the harmonic potential. The octupole potential is

$$\Phi^{(4)} = \frac{\Phi_0^{(4)}}{4R^2} \frac{a_{40}}{a_{20}} [(3-\varepsilon' + \varepsilon'')x^4 + (3+\varepsilon' + \varepsilon'')y^4 + 8z^4 + 6(1-\varepsilon'')x^2y^2 - 6(4+\varepsilon')y^2z^2 - 6(4-\varepsilon')x^2z^2], \quad (5)$$

where $\varepsilon' = a_{42}\sqrt{40}/a_{40}$ and $\varepsilon'' = a_{44}\sqrt{70}/a_{40}$. Any higher order potential $\Phi^{(k>2)}$ couples ionic motion along different axes, which leads to complicated nonlinear resonances³². Thus, a nearly pure quadrupole potential is necessary for a stable confinement of the ions.

The equation describing motion of the ion is

$$\frac{d^2}{dt^2} \begin{pmatrix} x \\ y \\ z \end{pmatrix} - V_{\text{T}}(t) \frac{Q}{mR^2} \begin{pmatrix} x \\ y \\ -2z \end{pmatrix} = 0, \quad (6)$$

which can be expressed in the form of Mathieu differential equation in terms of dimensionless parameters $\tau = \omega_{\text{rf}}t/2$, $a_{x,y} = -a_z/2 = -4QU/m\omega_{\text{rf}}^2R^2$ and $q_{x,y} =$

$-q_z/2 = 2QV/m\omega_{\text{rf}}^2R^2$. Solutions of eq. (6) follow from the Floquet theorem^{33,34} in terms of stability parameter $\beta_u(a_u, q_u)$ for $u \in \{x, y, z\}$. Under the adiabatic approximation $|a_u|$ and $q_u \ll 1$, which is achieved when the rf-electric field is homogeneous over the oscillation of the ion²⁸, the stability parameter reduces to $\beta_u \approx \sqrt{a_u + q_u^2}/2$. Then the approximate trajectory of the ion is

$$u(t) = C \cos\left(\beta_u \frac{\omega_{\text{rf}}}{2} t\right) \left[1 - \frac{q_u}{2} \cos(\omega_{\text{rf}}t)\right], \quad (7)$$

where C depends on the a_u and q_u values. The ion oscillates harmonically at frequency $\omega_{s,u} = \beta_u\omega_{\text{rf}}/2$, which is called secular or macro-motion. A faster oscillation which is smaller in amplitude is superimposed to the macro-motion. It is at the driving rf and is known as micro-motion. The amplitude of this motion increases as the ion goes further away from the trap centre³⁵. Hence confining ions within the sub-wavelength spatial extension is important to reduce systematic uncertainties related to micro-motion. Our trap is designed for $\omega_{\text{rf}} \sim 15$ MHz, though the actual value of ω_{rf} will depend on the loaded condition of the helical resonator as described later in the text.

We shall operate our trap at $U \approx 0$ V, which simplifies interpretation of the unstable q_u due to nonlinear resonances³⁶. At $a_u = 0$ and $\beta_u = q_u/\sqrt{2}$, the oscillating ion feels a time-averaged trapping in 3D. The effective ponderomotive potential

$$U_p(V, \omega_{\text{rf}}) = \frac{Q^2}{4m\omega_{\text{rf}}^2} \nabla\Phi(V)^2, \quad (8)$$

corresponds to depths $D_z = 2D_{x,y} = mz_0^2\omega_{\text{rf}}^2/q_z^2/16Q$ along axial and radial directions respectively. Here $2z_0$ is the separation between tips of two end-cap electrodes and r_0 is their radius. For an efficient capture, the rf-voltages will be such that trap depth is ten times larger than the initial energy of the ions.

Electrodes of our trap will be made out of tantalum due to its inert nature. The end-cap electrodes are made out of 1 mm diameter rods with their edges machined in conical shape at an angle 12° , as shown in Figure 1a. The concentric shielding electrodes will be built from tubes of inner and outer diameters 1.4 and 2 mm respectively. Edges of the

shielding electrodes will also be machined to an angle of 35° . In our optimized geometry tip of the end-caps and shielding electrodes will be separated by 0.6 and 1 mm respectively. We have simulated electric field lines of our trap geometry using a commercial software³⁷. The calculated potentials along different directions are shown in Figure 1 b and c). The potentials are fitted to an anharmonic function

$$f(u) = C_0 + \frac{c_2}{u_0^2}u^2 + \frac{c_4}{u_0^4}u^4, \quad (9)$$

where c_k are coefficients for k th-order multipole potential and u_0 is radius of the effective trap region along that direction. This assumes that the dominant perturbation of the harmonic potential is due to octupole term as given in eqs (4) and (5) respectively. We have estimated anharmonicity of our trap geometry $c_4/c_2 = 0.017$ and 0.092 along the axial and radial directions respectively.

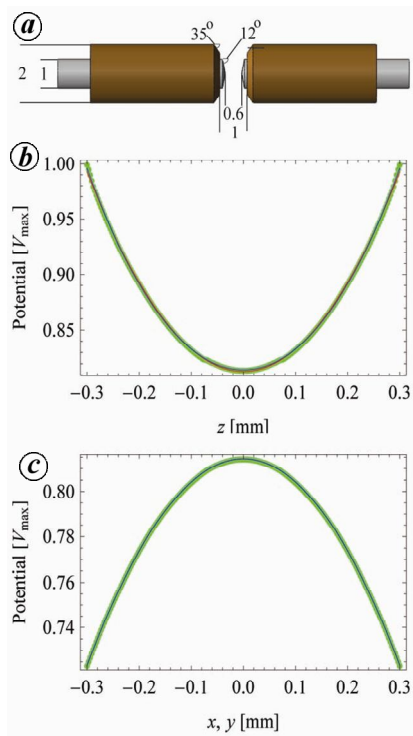


Figure 1. (a) Electrode geometry of the end-cap trap design (dimensions in mm). Potentials of the end cap-trap along (b) axial and (c) radial directions: normalized to maximum applied voltage V_{\max} . CPO software generated potential profiles (green) are fitted with harmonic (red) and anharmonic (blue) functions.

Helical rf-resonator

A narrow-bandwidth rf at large amplitude, ~ 1 kV peak-to-peak, is required for efficient trapping. Otherwise, it will result in unstable trapping and unwanted heating of the ions. Direct delivery of high-voltage rf to a trap damages the source due impedance mismatch between source and the trap electrodes. We have constructed an electromagnetically shielded resonator as shown in Figure 2, which inductively couples the rf source to the ion trap following the concept described in ref. 38. The resonator is constructed out of a copper tube which is wound in a helical shape (secondary coil) and placed inside a larger diameter copper tube for rf shielding. The farthest end of the secondary coil is grounded through the surface of the shielding tube and the other end couples rf to the trap. An antenna coil (primary) is positioned coaxially farther away from the grounded end of the secondary coil. The coupling efficiency to the secondary coil depends on the construction parameters as given in Table 1. The resonant frequency $f_0 = 2\pi/\sqrt{LC}$ of the resonator is determined by inductance L of the secondary coil and effective capacitance C . In



Figure 2. Primary (a) and secondary (b) coils of the rf-resonator which are attached to the cap and to the shielding tube of the resonator respectively. The secondary coil is placed coaxial to the shielding tube using some nonconducting spacers.

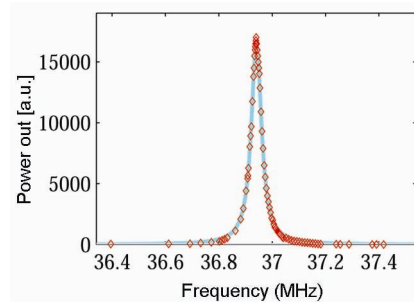


Figure 3. Frequency response of the unloaded rf-resonator (red) fitted to a Lorentzian spectrum (cyan). The grey line indicates input power to the resonator.

unloaded condition, C results from the distributed capacitance in the coil, capacitance between the secondary coil and the shielding. Capacitance between the trap electrodes adds up when the resonator is connected to the ion trap (loaded). The unloaded resonant frequency of our prototype resonator is $f_0 = 36.94(5)$ MHz and full width half maxima $\Delta f = 0.046$ MHz as shown in Figure 3. This has quality factor $Q = f_0/\Delta f = 800(20)$, which is required for delivering the rf to the trap at a cost of low power dissipation.

Energy levels of $^{171}\text{Yb}^+$

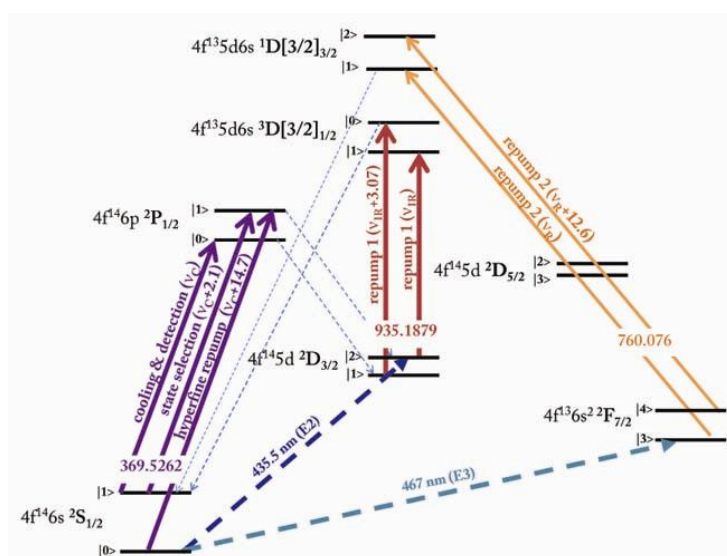
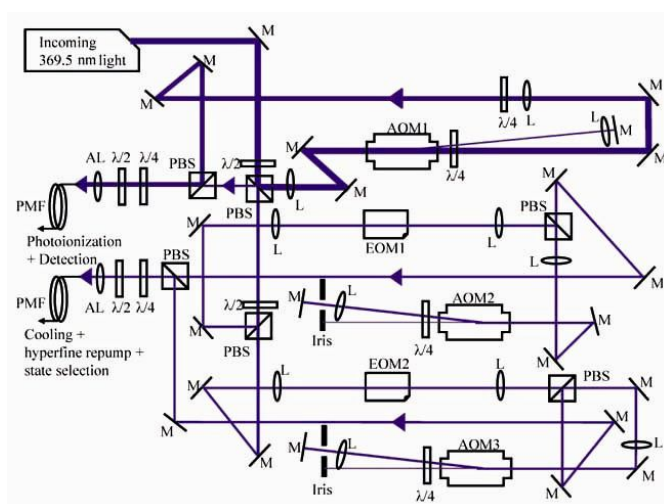
Laser cooling will be implemented to confine the ion within the Lamb Dicke regime³⁹, which is particularly important for precision frequency measurement, since it cancels out the first-order Doppler shift. The energy levels of $^{171}\text{Yb}^+$ relevant to our experiment and clock transitions are shown in Figure 4. The strong $|^2S_{1/2}; F=1\rangle - |^2P_{1/2}; F=0\rangle$ transition at wavelength 369.5262 nm will be driven for laser cooling the ion. The off-resonant scattering at wavelength 369.5262 nm populates the $F=0$ ground state. Transferring ions from this state to the cooling cycle requires a light which is 14.7 GHz upshifted from the cooling laser. The $|^2P_{1/2}; F=1\rangle$ state has branching once in every 200 cycles to the metastable $^3D_{3/2}$ states. A pair of lasers separated by 3.07 GHz at wavelength 935.1879 nm is required for depopulating the $^3D_{3/2}$ states via the $|^3D[3/2]_{1/2}; F=1, 2\rangle$ states. In spite of no direct branching, ion cascades to the long-lived $|^2F_{7/2}; F=3, 4\rangle$ states due to collision with background gases. This limits the ion interrogation time even though the trap lifetime is very long. Repump lasers at wavelength 760.076 nm are needed to drive the $|^2F_{7/2}; F=3\rangle - |^1D[3/2]_{3/2}; F=1\rangle$ and $|^2F_{7/2}; F=4\rangle - |^1D[3/2]_{3/2}; F=2\rangle$ E2-transitions separated by 12.6 GHz. The $|^2S_{1/2}; F=1\rangle - |^2P_{1/2}; F=1\rangle$ transition will be driven to optically pump the ion to the $F=0$ ground state. This state preparation requires a 2.1 GHz blue detuned light from the cooling laser before probing the clock transition.

Optical set-up

In this section we will describe the proposed optical arrangements of the lasers for photoionization and cooling. The

Table 1. Design parameters of the rf-resonator

	Part	Dimension
Tube for secondary coil	Outer diameter	6 mm
	Inner diameter	2 mm
Secondary coil	Outer diameter	60 mm
	Length	95 mm
	Number of turns	8.5
	Pitch	3.8 mm
Wire for primary coil	Outer diameter	2.4 mm
	Primary coil	Outer diameter
Shielding tube	Number of turns	2.5
	Pitch	3.8 mm
	Length	160 mm


Figure 4. Lowest lying energy levels of $^{171}\text{Yb}^+$ relevant frequency standards (dashed lines) and laser cooling (solid lines). Branching from the excited states is shown as dotted lines. Wavelengths and hyperfine splittings are in nm and GHz respectively.

Figure 5. Optical arrangement of 369.5363 nm laser for generating photoionization, cooling, detection, hyperfine repumping and optical pumping lights. Mirrors (M), lens (L), polarizing beam splitter (PBS), $\lambda/4$ ($\lambda/2$) quarter (half) waveplates, aspheric lens (AL) and polarization maintaining single-mode fibre (PMF) are shown.

two-step photoionization process⁴⁰ for producing $^{171}\text{Yb}^+$ consists excitation of the ^{171}Yb atom to the $^1\text{P}_1$ state using light from a commercial extended cavity diode laser (ECDL) (SYST Blue Tune, Toptica Photonics AG)⁴¹ at wavelength 398.9 nm. In the next step energy >3.15 eV is required to strip out one valence electron from the excited ^{171}Yb . An intense part of the cooling laser light will be used for this. For isotope selective photoionization, elliptical-shaped lights will coincide vertically with the Yb atomic beam.

A frequency-doubled ECDL system will produce the 369.5262 nm light (TA-SHG Pro, Toptica Photonics AG)⁴¹. A large fraction of it passes through a 200 MHz acousto-optic modulator (AOM) AOM3 (46200-6-1-.37-XQ, Gooch and Housego)⁴¹ as shown in Figure 5. The zeroth-order will be used for photoionization and the double-passed first-order will be used for fluorescence detection. A 14.7 GHz blue detuned sideband will be generated from rest of the light by taking the second-order sideband of a 7.37 GHz electro-optic modulator (EOM) EOM2 (4851-M, Newport Corp.)⁴¹. For fine-tuning of the frequency and controlling the optical power, EOM2 output will be double-passed through a 200 MHz AOM2 (46200-6-1-.37-XQ, Gooch and Housego)⁴¹. Remaining light will be used for the state selection which will be produced by using a combination of 2.1 GHz EOM1 (4431-M, Newport Corp.) and double passing through 200 MHz AOM1 (46200-6-1-.37-XQ, Gooch and Housego)⁴¹.

A pair of ECDLs at wavelengths 935.1879 nm (DL Pro, Toptica Photonics AG)⁴¹ and 760.076 nm (DL 100 Pro, Toptica Photonics AG)⁴¹ will be used for repumping. Output of the lasers will be coupled to EOMs operating at 3.07 GHz and 12.6 GHz (Fiber EOM, Photline Tech.)⁴¹ for 935.1879 and 760.076 nm lasers respectively. In addition, double passing of the first-order through AOMs (46200-.2, Gooch and Housego)⁴¹ will be used for frequency tuning and fast switching of these lights.

Conclusion

In this article we have described the design of an end-cap ion trap. The numerically calculated trapping potentials are nearly harmonic, which is suitable for precision measurement of frequency. The

high quality factor rf-resonator is ready for delivering AC voltage to the trap. We have also described optical arrangements for the photoionized production of ions and their laser cooling. Trapped $^{171}\text{Yb}^+$ in this facility will be used for the first optical frequency standard in India.

1. Webb, J. K., Flambaum, V. V., Churchill, C. W., Drinkwater, M. J. and Barrow, J. D., *Phys. Rev. Lett.*, 1999, **82**, 884–887.
2. Rosenband, T. *et al.*, *Science*, 2008, **319**, 1808–1812.
3. Fischer, M. *et al.*, *Phys. Rev. Lett.*, 2004, **92**, 230802.
4. Blatt, S. *et al.*, *Phys. Rev. Lett.*, 2008, **100**, 140801.
5. Chou, C. W., Hume, D. B., Rosenband, T. and Wineland, D. J., *Science*, 2010, **329**, 1630–1633.
6. Diddams, S. A., Bergquist, J. C., Jefferts, S. R. and Oates, C. W., *Science*, 2004, **306**, 1318–1324.
7. Guéna, J. *et al.*, *IEEE Trans. Ultrasonics, Ferroelectrics, Frequency Control*, 2012, **59**, 391–410.
8. Allan, D. W., *Proc. IEEE*, 1966, **54**, 221–230.
9. Dehmelt, H. G., *IEEE Trans. Instrum. Meas.*, 1982, **31**, 83–87.
10. Derevianko, A. and Katori, H., *Rev. Mod. Phys.*, 2011, **83**, 331–347.
11. Takamoto, M., Hong, F.-L., Higashi, R. and Katori, H., *Nature*, 2005, **435**, 321–324.
12. Hinkley, N. *et al.*, *Science*, 2013, **341**, 1215–1218.
13. Nicholson, T. L. *et al.*, *Phys. Rev. Lett.*, 2012, **109**, 230801.
14. Th. Udem, Diddams, S. A., Vogel, K. R., Oates, C. W., Curtis, E. A. and Lee, W. D., *Phys. Rev. Lett.*, 2001, **86**, 4996–4999.
15. Chr. Tamm, Weyers, S., Lipphardt, B. and Peik, E., *Phys. Rev. A*, 2009, **80**, 043403.
16. Barwood, G. P., Margolis, H. S., Huang, G., Gill, P. and Klein, H. A., *Phys. Rev. Lett.*, 2004, **93**, 133001.
17. Huntemann, N., Okhapkin, M., Lipphardt, B., Weyers, S., Tamm, Chr. and Peik, E., *Phys. Rev. Lett.*, 2012, **108**, 090801.
18. Dubé, P., Madej, A. A., Zhou, Z. and Bernard, J. E., *Phys. Rev. A*, 2013, **87**, 023806.
19. Gao KeLin, *Chin. Sci. Bull.*, 2013, **58**, 853–863.
20. Wanga, Y. H. *et al.*, *Opt. Commun.*, 2007, **273**, 526–531.
21. Chou, C. W., Hume, D. B., Koelemeij, J. C. J., Wineland, D. J. and Rosenband, T., *Phys. Rev. Lett.*, 2010, **104**, 070802.
22. Champenois, C., Houssin, M., Lisowski, C., Knoop, M., Hagel, G., Vedel, M. and Vedel, F., *Phys. Lett. A*, 2004, **331**, 298–311.
23. Versolato, O. O., Wansbeek, L. W., Jungmann, K., Timmermans, R. G. E., Willmann, L. and Wilschut, H. W., *Phys. Rev. A*, 2011, **83**, 043829.
24. Dzuba, V. A. and Flambaum, V. V., *Phys. Rev. A*, 2008, **77**, 012515.
25. Margolis, H. S., *Contemp. Phys.*, 2010, **51**, 37–58.
26. Paul, W., Osberghaus, O. and Fischer, E., *Forschungsbe Wirtsch.-Verkehrminist. Nordrhein-Westfalen*, 1958, 415.
27. Penning, F. M., *Physica*, 1936, **3**, 873–1052.
28. Major, F. G., Gheorghe, V. N. and Werth, G., *Charged Particle Traps, Springer Series on Atomic, Optical and Plasma Physics*, Springer, 2010.
29. Bennewitz, H. G. and Paul, W., *Z. Phys.*, 1954, **139**, 489–492.
30. Neuhauser, W., Hohenstatt, M. and Toschek, P., *Phys. Rev. Lett.*, 1978, **41**, 233236.
31. Schrama, C. A., Peik, E., Smith, W. W. and Walther, H., *Opt. Commun.*, 1993, **101**, 32–36.
32. Wang, Y., Franzen, J. and Wanczek, K. P., *Int. J. Mass Spectrom. Ion Process.*, 1993, **124**, 125–144.
33. Abramowitz, M. and Stegun, I. A., *Handbook of Mathematical Functions*, NBS Applied Mathematics Series No. 55, 1972.
34. McLachlan, N. W., *Theory and Applications of Mathieu Functions*, Oxford, 1947.
35. Eschner, J., Morigi, G., Schmidt-Kaler, F. and Blatt, R., *J. Opt. Soc. Am.*, 2003, **20**, 1003–1015.
36. Alheit, R., Kleineidam, S., Vedel, F., Vedel, M. and Werth, G., *Int. J. Mass Spectrom. Ion Process.*, 1996, **154**, 155–169.
37. 3D charged particle optics program (CPO-3D), CPO Ltd, USA.
38. Siversns, J. D., Simkins, L. R., Weidt, S. and Hensinger, W. K., *Appl. Phys. B*, 2012, **107**, 921–934.
39. Eschner, J., Morigi, G., Schmidt-Kaler, F. and Blatt, R., *J. Opt. Soc. Am. B*, 2003, **20**, 1003–1015.
40. Sankari, M. and Suryanarayana, M. V., *J. Phys. B: At. Mol. Opt. Phys.*, 1998, **31**, 261–273.
41. CSIR-NPL does not endorse these models but the specification matches with the experimental requirement.

ACKNOWLEDGEMENTS. We thank Chr. Tamm and P. Mandal for useful discussions. This work was carried out as a part of Single Trapped Ion Optical Standard (STIOS) programme funded by CSIR-NPL, New Delhi.

Received 26 November 2013; revised accepted 28 March 2014

S. De*, N. Batra, S. Chakraborty, S. Panja and A. Sen Gupta are in the CSIR-National Physical Laboratory, Dr K. S. Krishnan Marg, New Delhi 110 012, India.
*e-mail: subhadeep@mail.nplindia.org